

Analysis of the small-angle intensity scattered by a porous and granular medium

Scattering by Powders:

small-angle - X-ray - scattering
(SAXS):

$$I_{\text{Abs}} = \frac{1}{V} \frac{d\sigma(\vec{u})}{d\Omega} = \frac{C}{C_0 \Delta S \text{Fe}_s}$$

consider sample of thickness e_s , which is homogeneous on macroscopic scale but contains two phases: φ_s and $\Sigma (\text{m}^{-1})$ can be extracted from scattered intensity

$$Q = \int_0^{\infty} I_{\text{Abs}} q^2 dq = 2\pi^2 \varphi_s (1-\varphi_s) (\Delta S)^2$$

$$\Sigma = [\lim_{q \rightarrow \infty} (I_{\text{Abs}} q^4)] / [2\pi (\Delta S)^2]$$

↑ Porod limit (due to well defined and smooth interface between two phases, not always reached (especially for rough interface))

Scattering often calls for very thin layers to avoid absorption and/or multiple scattering at small angles
→ e_s can not be measured macroscopically

→ Σ (sample specific surface) is often scaled by sample volume and not by solid volume → irrelevant result. → use C instead

\vec{u} : direction

$d\sigma(\vec{u})$: differential scattering cross-section

V : Volume of illuminated sample

I_{Abs} : absolute (or scaled) intensity

C_0 : incoming flux of photons on the sample

C : number of photons collected per second in ΔS

ΔS : solid angle

T : sample transmission

e_s : sample macroscopic thickness

Δg : electronic contrast of two sample phases

φ_s : volume fraction of solid phase

Σ : total quantity of interface between two phases (m^{-1}).

Q : "invariant"

q : scattering vector (in $\frac{1}{\text{Å}}$)

$$\varphi^* = \frac{V_e}{V}$$

"envelope" of a grain is not always straight forward, but can be done easily when system presents two length scales: nanopores (a few nanometers) and micrometric grains \rightarrow smooth external grain border

$$\varphi = \frac{V_i}{V_e}$$

$$\Rightarrow \text{th. } \frac{V_s}{V_e} = 1 - \varphi$$

$$\Rightarrow \varphi_s = \varphi^* (1 - \varphi)$$

φ is an intrinsic property of the material
 φ_s depends on the sample compactness

if pores are much smaller than grains,
 Σ arises mainly from inner porosity

Σ includes inner porous surface \rightarrow clear and unambiguous definition.

Σ_e results from smoothing

$$\Sigma = \frac{S}{V}, \quad \Sigma_e = \frac{\Sigma_e}{V}$$

(here $\Sigma \gg \Sigma_e$)

Σ and Σ_e are useful when φ^* is unknown \rightarrow better scale by V_s or V_e of grains

Σ_s, φ and $\Sigma_{e,G}$ are used to characterise porous and granular media

φ^* : compactness of the sample

V_e : volume of the envelopes of the sample grains

V : Volume of the sample

V_i : total volume of pore contained in V_e

φ : inner porosity

V_s : Volume of solid

φ_s : solid volume fraction

S : total amount of interface of the grains

Σ_e : total amount of envelope surface of the grains

$$\Sigma_s = \frac{S}{V_s} = \frac{\Sigma}{\varphi^* (1 - \varphi)}$$

$$\Sigma_{e,s} = \frac{\Sigma_e}{V_s} = \frac{\Sigma_e}{\varphi^* (1 - \varphi)}$$

$$\Sigma_G = \frac{S}{V_e} = \frac{\Sigma}{\varphi^*}$$

$$\Sigma_{e,G} = \frac{\Sigma_e}{V_e} = \frac{\Sigma_e}{\varphi^*}$$

Σ : scattering length density of the solid

μ_{solid} : absorption coefficient of the solid

Σ_s : scattering length density of the solvent

μ_{solvent} : absorption coefficient of the solvent

Case (i): air in the inner pores and the inter-grains porosity

e_B can be calculated from the measured transmission:

$$e_B = - \frac{\ln(T)}{\mu_{\text{solid}}} = e_s \varphi^* (1-\varphi)$$

T measured as ratio of beam flux transmitted by sample to flux transmitted by empty cell.

μ_{solid} calculated from composition of dry sample powder

$$I_1 = \frac{C}{C_0 \Delta \Omega T e_B} = \frac{I_{\text{abs}}}{\varphi_s}$$

Case (ii): solvent in the inner pores and air in the inter-grains porosity

$$e_H = - \frac{\ln(T)}{\mu_{\text{grain}}} = e_s \varphi^*$$

e_H is average thickness of material (solid + inner pore) on the beam path

$$\mu_{\text{grain}} = \mu_{\text{solid}} (1-\varphi) + \mu_{\text{solvent}} \varphi$$

e_B and e_H are not equal even if the pores are empty of solvent

calculation of μ_{grain} uses assumption for φ
 → when φ is determined in the end, the result must be checked for consistency → iterative cycle

$$I_2 = \frac{C}{C_0 \Delta \Omega T e_H} = \frac{I_{\text{abs}}}{\varphi^*}$$

e_B : apparent thickness (sample)

I_1 : "measurable" intensity

e_H : apparent thickness (sample)

μ_{grain} : absorption coefficient of the grains

I_2 : "measurable" intensity

case (iii): solvent in the inner and inter-grains porosity

When sample can be made thick enough ~~thin~~ by dilution (e.g. solvent contains slight amount of xanthan gum to suspend grains), thickness can be measured correctly $\Rightarrow I_{\text{Abs}}$ measurable

Ψ_s can be deduced from known material densities (weighing large amounts of wet and dry samples)

works only well, when "paste" is homogenous w.r.t. beam size

When beam size is very small (few 100 μm) other solution: deduce Ψ_s from transmission of the sample

transmission of the wet paste:

$$T = e^{-\mu_{\text{paste}} \cdot e_s}$$

μ_{paste} : absorption coefficient of wet sample paste

$$\begin{aligned}\mu_{\text{paste}} &= \Psi_s \mu_{\text{solid}} + (1 - \Psi_s) \mu_{\text{solvent}} \\ &= \Psi^* (1 - \Psi) \mu_{\text{solid}} + (1 - \Psi^* (1 - \Psi)) \mu_{\text{solvent}} \\ &= \Psi^* (1 - \Psi) \mu_{\text{solid}} + (1 - \Psi^* + \Psi^* \Psi) \mu_{\text{solvent}} \\ &= \frac{V_e}{V} (1 - \frac{V_i}{V_e}) \mu_{\text{solid}} + (1 - \frac{V_e}{V} + \frac{V_e}{V} \cdot \frac{V_i}{V_e}) \mu_{\text{solvent}} \\ &= \frac{V}{V} [(V_e - V_i) \mu_{\text{solid}} + (V - V_e + V_i) \mu_{\text{solvent}}]\end{aligned}$$

I_1 : intensity scaled to solid content

$$I_1 = \frac{I_{\text{Abs}}}{\Psi_s} = I_{\text{Abs}} \cdot \frac{V}{V_e - V_i}$$

? Question: That way the intensity grows. Does that value make any sense physically?

Experimental:

Correct measurement of scattered intensity requires very large range of scattering vector ($3 \times 10^{-4} \text{ \AA}^{-1}$ to 1 \AA^{-1})
→ usually different setups have to be coupled.

camera installed on source
↓

Lab: either conventional 2D Guinier camera (Mo source delivers high-energy photons, $\lambda = 0.71 \text{ \AA}$) or Huxley-Holmes camera (rotating anode with Cu target)

→ q from 1 \AA^{-1} to 1 \AA^{-1} = SAXS

USAXS: 1-D camera with two Ge channel-cut crystals in Bonse-Hart geometry (rotating Cu anode delivers photons with $\lambda = 1.54 \text{ \AA}$)

→ q range: $3 \times 10^{-4} \text{ \AA}^{-1}$ to 0.01 \AA^{-1}

Vertical geometry of machine is linear → photons need to be desmeared (Strobel's method used)

? Question: What does "desmear" mean? Why?

Wide range of q gives information about heterogeneities in the sample ranging from a few Ångströms to a few micrometres.
(very good for material with two different length scales).

I_1 and I_2 are obtained by controlling sample transmission, solid angle of experiment and incoming flux. No secondary standards required.

? Question: What does "solid angle" mean?

True scaled intensity I_{Abs} can only be obtained, when sample thickness can be measured.

Data background corrected (to eliminate scattering from solvent, e.g.)
Beam is a few mm^2 wide at sample position

Some experiments performed on Beamline BM02 (French CRG) at ESRF in Grenoble

Model for data treatment:

three regimes observed:

(I) Porod regime at low q values $q < 0,005 \text{ Å}^{-1}$ \rightarrow envelopes

(II) transition regime $0,005 \text{ Å}^{-1} < q < 0,03 \text{ Å}^{-1}$

(III) Porod regime at high q values $q > 0,03 \text{ Å}^{-1}$ \rightarrow inner pores

(Porod regime means linear decay in plot $\log(I)$ vs. $\log(q)$)

Determination of Ψ by the invariant Q :

"rearrange" granular layer into double layer:

one contains material: thickness e_H , inner porosity Ψ

one contains only solvent and/or air: thickness $e_S - e_H$

\rightarrow low q scattering disappears (corresponds to outer envelopes of grains)

$$I_{\text{Abs}}^{\text{corr}} = I_{\text{Abs}} - I_{\text{Abs}}(q_k) \cdot \frac{q^4}{q_k^4} \quad \leftarrow \begin{matrix} \text{integral} \\ \text{over } q_k? \end{matrix}$$

$$\Rightarrow I_1^{\text{corr}} = \frac{I_{\text{Abs}}^{\text{corr}}}{\varphi^* \cdot (1-\Psi)} \quad I_2^{\text{corr}} = \frac{I_{\text{Abs}}^{\text{corr}}}{\varphi^*}$$

$I_{\text{Abs}}^{\text{corr}}$: absolute intensity of only grains and solvent/air layers
 q_k : any value of q in regime (I)

$I_{\text{Abs,mat}}$: absolute intensity of the material layer

? Question: I_2^{corr} (and V_e) contain by definition the envelope of the grain and the solvent in the inner pores of the grain. Why should the material in the inner pores contribute to the intensity of the material layer?

Material layer:

$$Q = \int_0^\infty I_{\text{Abs,mat}} q^2 dq = 2\pi^2 \varphi (1-\varphi) \Delta g^2$$

case (i): $\Delta g = g$

case (ii) & (iii): $\Delta g = g - g_s$

\Rightarrow case (i): $Q = \int_0^\infty I_1^{\text{corr}} q^2 dq = 2\pi^2 \varphi g^2$

case (ii): $Q = \int_0^\infty I_2^{\text{corr}} q^2 dq = 2\pi^2 \varphi (1-\varphi) (g-g_s)^2$

case (iii): $Q = \int_0^\infty I_1^{\text{corr}} q^2 dq = 2\pi^2 \varphi (g-g_s)^2$

Question: Why do they now go back to I_1^{corr} and I_2^{corr} when they just claimed that $I_{\text{Abs,mat}}$ is always $I_2^{\text{corr}}/2$.

Experimentally, the calculation of the $\int \dots dq$ requires an extrapolation of I_1^{corr} and I_2^{corr} in the region (II), where they cannot be accessed experimentally.

\rightarrow assume constant value in this case (first significant value for lowest q in region (II))

$\sim \varphi$ can be accessed without knowing φ^* and real sample thickness.

in case (ii) results have to be cycled until self-consistent.

Determination of the specific surface of pores from high- q Porod law: (region (III))

Asymptotic limit of Porod's law can be obtained by plotting Iq^4 vs q (Porod plot/representation).

High- q domain: specific surface corresponds to interface between pores and bulk material

$$\text{case (i): } \Sigma_s = \frac{1}{\psi^*(1-\psi)} \frac{\lim_{q \rightarrow \infty} (I_{\text{abs}} q^4)}{2\pi (g - g_s)^2} = \frac{\lim_{q \rightarrow \infty} (I_1 q^4)}{2\pi (g - g_s)^2}$$

$$\text{case (ii): } \Sigma_s = \frac{1}{\psi^*} \frac{\lim_{q \rightarrow \infty} (I_{\text{abs}} q^4)}{2\pi (g - g_s)^2} = \frac{\lim_{q \rightarrow \infty} (I_2 q^4)}{2\pi (g - g_s)^2}$$

$$\text{case (iii): } \Sigma_s = \frac{\lim_{q \rightarrow \infty} (I_1 q^4)}{2\pi (g - g_s)^2}$$

I_1 and I_2 are directly measurable.

Specific surface is often expressed in $\frac{m^2}{g} \rightarrow$ divide ~~divide by Σ_{sig}~~ Σ_{sig} by the density of the solid $\rho_m (\frac{g}{m^3})$.

Determination of S_e/V_e from low- q Porod law (region (II))

Apply same method as above.

Scattering arises from contrast Δg^* between air or solvent and grains

$$\text{case (i): } \Delta g^* = (1-\psi)g$$

$$\text{case (ii): } \Delta g^* = (1-\psi)g + \psi g_s$$

$$\text{case (iii): } \Delta g^* = (1-\psi)(g - g_s)$$

$$\text{case (i): } \Sigma_{eig} = \frac{1}{\psi^*} \frac{\lim_{q \rightarrow 0} (I_{\text{abs}} q^4)}{2\pi (\Delta g^*)^2} = \frac{\lim_{q \rightarrow 0} (I_1 q^4)}{2\pi g^2 (1-\psi)}$$

$$\text{case (ii): } \Sigma_{eig} = \frac{1}{\psi^*} \frac{\lim_{q \rightarrow 0} (I_{\text{abs}} q^4)}{2\pi (\Delta g^*)^2} = \frac{\lim_{q \rightarrow 0} (I_2 q^4)}{2\pi [(1-\psi)g + \psi g_s]^2}$$

$$\text{case (iii): } \Sigma_{eig} = \frac{1}{\psi^*} \frac{\lim_{q \rightarrow 0} (I_{\text{abs}} q^4)}{2\pi (\Delta g^*)^2} = \frac{\lim_{q \rightarrow 0} (I_1 q^4)}{2\pi (g - g_s)^2 (1-\psi)}$$

Δg^* : contrast between air or solvent and grains

Scattering by a porous grain:

Formulae above do not suppose anything about geometric repartition of the porous surface inside the grains but that the grain is homogeneously porous.

Now assume:

- all grains identical and globular with volume V
- each grain contains n pores of volume v

V : volume of individual grain

n : number of pores

Scattering intensity is Fourier transform of the correlation

function between two elementary volumes i and j located in the complementary region of the solid.

Separate three contributions:

a) i and j located outside grain envelope

b) i and j located inside grain

c) i inside and j outside grain

scattering intensity:

$$a) I_a = (\rho_{out} - \rho)^2 V^2 F_0^2(q) = (\rho_{out} - \rho)^2 V^2 P_0(q)$$

$$b) I_b = (\rho - \rho_{in})^2 n v^2 f_0^2(q) [S(q) + (n-1) P_0(q)]$$

$$c) I_c = -2(\rho_{out} - \rho)(\rho_{in} - \rho) n v V P_0(q) f_0(q)$$

ρ_{out} : scattering length density inside grain

v : volume of each pore

$f_0(q)$: amplitude of the form factor

porosity

$P_0(q)$: normalized intensity of the form factor

of an homogeneous grain

global intensity is sum of all three contributions:

~~consider N grains with macroscopic volume fraction~~

Ψ^* and uncorrelated cores ($S(q) = 1$ for all q).

$$\rightarrow I_{abs} = \Psi^* \left\{ \Psi v f_0^2 (\rho - \rho_{in})^2 + V P_0 [(\rho - \rho_{out})^2 \right.$$

$$- 2\Psi f_0 (\rho_{out} - \rho)(\rho_{in} - \rho) \right.$$

$$\left. + \Psi^2 f_0^2 (\rho - \rho_{in})^2] \right\}$$

Ψ : scattering length density inside pore

ρ_{in} : scattering length density inside pore

$f_0(q)$: amplitude of the form factor

of an homogeneous grain

$P_0(q)$: normalized intensity of the form factor

of an homogeneous grain

ρ : scattering length density outside grain

ρ_{out} : scattering length density outside grain

this leads to both Porod limits (high and low q) without any approximation in all cases (i) to (iii)

$f_0(q)$: normalisation amplitude

discuss approximation made in the determination of the invariant Q (splitting sample in material layer and solvent + air layer):

$f_0 = 1$ in region I ~~for small pores~~

N : number of grains

$$\Rightarrow I_{\text{abs}} \Big|_{q \approx 0} \approx \varphi^* V P_0 \left[(g - g_{\text{out}})^2 - 2\varphi (g_{\text{out}} - g) \cdot (g_{\text{in}} - g) + \varphi^2 (g - g_{\text{in}})^2 \right]$$

$$\Rightarrow I_{\text{abs,mat}} \approx \varphi v f_0^2 (g - g_{\text{in}})^2 + V P_0 \left[-2\varphi (f_0 - 1) \cdot (g_{\text{out}} - g) \cdot (g_{\text{in}} - g) + \varphi^2 (f_0^2 - 1) (g - g_{\text{in}})^2 \right]$$

the correction this term contains w.r.t. the term before can be neglected as long as the ratio of size between the grain and the pores is high enough (more than 10).

In that case P_0 is negligible in regions (II) and (III).

Examples of application:

maybe later

Mitterdorfer et al. 2014

Small-angle neutron scattering study of micropore collapse in amorphous solid water

Amorphous Solid Water (ASW) in space:

- Vapour deposited ASW is the most abundant solid molecular material in space.
- plays a direct role in formation of more complex chemical species and in aggregation of icy materials in the earliest stages of planet formation
- does not naturally form on earth (except coldest region of atmosphere ($T < 150\text{ K}$, altitude $\approx 80\text{ km}$))
- most widespread occurrence: • on interstellar dust, • in comets, • in many solar system bodies
- accretes onto dust particles in cold regions of dense interstellar clouds
- acts as reservoir trapping volatile gases \rightarrow key role in promoting chemical reactions
- may be pivotal in earliest stages of planet formation
- formation paths on interstellar dust particles:
 - chemical vapour deposition at 10 K , involving reaction of $\text{O}_2, \text{H}_2, \text{O}_2, \text{H}_2, \text{OH}$ (dominant in cold dark star-forming clouds)
 - direct water vapour deposition onto dust particles (dominant in shocked regions and disks)

Astrophysical implications from the results of this study:

- sudden 3D \rightarrow 2D transition may severely change the formation rate of H_2 from H atoms:
 - H -atom recombination is very efficient on single crystal surfaces but very inefficient on external surfaces of amorphous ice.

- in micropores the probability of an encounter between two H-atoms is greatly increased before pore collapse and even more so afterwards (H-atoms confined between lamellae)
- no possibility of desorption from lamellae → might be even more efficient than formation on single crystals
- Possibility of crystallizing clathrate hydrates in vacuo:
 - if micropores are originally filled with gases like CO, CO₂, CH₄, O₂ (e.g. in cometary nuclei)
 - these molecules will have a strong tendency to escape upon pore collapse, but no path to the exterior
 - internal pressure will build up
 - formation of clathrates becomes thermodynamically feasible in spite of the vacuum environment
- Complex organic chemistry:
 - high internal pressure after collapse may explain how complex organic compounds may form in relatively short amount of time in interstellar ices
 - these might be carried in comets and meteorites as suggested in "Late Bombardment" hypothesis for origins of life
 - formation of long chain-like molecules (e.g. interstellar polyynes) is strongly favoured when chemistry takes place in 2D lamellae.
- Attention: samples of study produced at 77 K
formation in space : 10-60 K

Sample preparation:

- ASW is similar (in terms of radial distribution functions) to hyperquenched glassy water (HGW) and low density ASW typical production conditions:
 - HGW: ultrafast cooling of liquid water droplets
 - ASW: water vapour deposition on cold substrates

- low density ASW: pressure-induced amorphization of ice at 77K and > 1.2 GPa (resulting in high density amorphous ice) followed by bringing the sample to ~ 140 K at 0-0.1 GPa
- morphology of ASW depends on deposition conditions:
flow rate, directionality, substrate temperature, water partial pressure
- when deposition temperature is increased from < 10 K to > 200 K deposited ice phases change from porous ASW to compact ASW to cubic to hexagonal ice
- same transition sequence is observed when ASW deposited at low temperature is heated
- bulk density of such ices (disregarding pores) is $0.93 \pm 0.01 \frac{g}{cm^3}$
at very low deposition temperatures ASW of higher bulk density may form

ASW production for this study:

- D₂O (99.8 Atom% D, Carl ROTH) deposited on a cold (77K) copper plate (direct contact with liquid nitrogen)
- background pressure: 1×10^{-4} mbar
- needle valve used to adjust D₂O pressure
 - slow deposition: 0.1 mbar D₂O \rightarrow 40 μ m/h growth rate
 - fast deposition: 0.3 mbar D₂O \rightarrow 130 μ m/h growth rate
- deposition times: between 24 and 30 hours
- two production modes:
 - baffled flow: background deposition
 - non-baffled, supersonic flow: line of sight deposition
- highly porous ASW (pASW) forms under these conditions
- after deposition, ASW was scraped off the copper plate under liquid nitrogen using a spatula
- stored as granular material in LN₂ and shipped to ISIS
- granules transferred into a null-scattering Ti₂T alloy cell under LN₂, compacted with spatula and placed into Helium cryostat immediately.

Experimental Methods and conditions:

- small angle neutron or X-ray scattering:
 - non-destructive
 - particularly suited to study granular and porous structures with dimensions between 10 and 1000 Å
- NIMROD can measure continuous length scale from <1 to >300 Å
 - measure small angle neutron scattering signal ($Q < 1 \text{ \AA}^{-1}$) simultaneously with large angle neutron scattering signal ($Q > 1 \text{ \AA}^{-1}$)
 - $Q < 1 \text{ \AA}^{-1}$: information on pore-structure → pore collapse
 - $Q > 1 \text{ \AA}^{-1}$: information on short-, intermediate- and long-range ordering of water molecules → crystallization

Sample treatment:

- held at 90 K for 30 min, recording scattering continually
- heat up 10 K (heating rate 0,3 K/min)
- collect data for another 30 min
- increase temperature to at least 160 K

Sample: surface: internal surface up to $230 \pm 10 \frac{\text{m}^2}{\text{g}}$
- quantity: few grammes

Data Analysis:

- split Q-range into two parts, below and above 1 \AA^{-1}

Intermediate Q-range (1 to 10 \AA^{-1}):

- for $T > 150$ K sharp Bragg peaks develop ~~develop~~
(e.g. [111], [220], [222], [331] cubic ice reflections)
- infer crystallization of amorphous material to cubic ice
(peaks get sharper towards higher temperatures)

Small-angle neutron scattering:

- high intensity in low- Q -range, due to heterogeneous nature of ASW matrix
- main feature is shoulder (hump/knee) at $\approx 0.1 \text{ \AA}^{-1}$ for all scattering curves recorded at $T < 120 \text{ K}$ but not at higher T
- shoulder indicates microporous nature, which disappears at higher temperatures
- model independent analysis:

- scattered intensity at small angles provides an absolute scale (in cm^{-1}) from which the specific surface area can be extracted:

Σ_s : specific surface area

K : Porod constant

ρ_m : mass density of the solid

Δg : difference between

Δg^2 : scattering contrast

scattering length densities of solid and

empty pores

- plot $I(Q) \cdot Q^4$ vs Q

→ data forms more or less a plateau between Q_1 and 0.3 \AA^{-1} (Porod regime)

→ "half-way" point of this plateau is taken for K
(which ideally should be $\lim_{Q \rightarrow \infty} (I(Q) \cdot Q^4)$)

$$\cdot \Sigma_s = \frac{1}{\rho_m} \cdot \frac{\lim_{Q \rightarrow \infty} (I(Q) Q^4)}{2\pi \Delta g^2} = \frac{1}{\rho_m} \cdot \frac{K}{2\pi \Delta g^2}$$

- to better determine presence and position of shoulder
plot $I(Q) \cdot Q^d$ vs Q

d is chosen in a way that the plot transforms the shoulder into a pronounced peak (2.5 or 3 in these cases)
→ "pseudopeak"

- apply models to data:

• none of the models assuming a spherical pore shape
(and e.g. a ~~flat-topped~~ Maxwellian size distribution)

is able to capture the features in the data or the ones known from literature.

new

* Guinier Porod model:

- * can capture the pore collapse features by allowing for non-spherical pores

- * sphericity factor s as indicator of pore shape:

$s = 0$: spherical pore

$s = 1$: cylindrical pore

$s = 2$: platelet

dimensionality parameter: $3-s$

- * use two fitting regions: Guinier region for $Q < Q_1$ (contains knee)

Porod region for $Q > Q_1$ (linear on double logarithmic I vs Q plot)

$$* I(Q) = \frac{G}{Q^s} \cdot e^{-\frac{Q^2 \cdot R_G^2}{3-s}}, Q \leq Q_1$$

$$I(Q) = \frac{D}{Q^d}, Q \geq Q_1$$

R_G : radius of gyration

G : Guinier scaling factor

d : Porod exponent

D : Porod scaling factor

- * Guinier region is dominated by contributions from the micropores

- * scattered intensities fitted up to 140 K
variance in fit parameters determines error bars

Results and previous works:

02.02.2015

General:

- The same structure transitions that are observed for forming ice at different temperatures are observed when breaking ice that was formed at low temperatures.
- collapse of pore network marking the transition from porous to compact ASW still not understood
- comparison of results from different labs not straight forward because of different deposition techniques and flow rates
→ different morphology, surface area, contamination levels

- ungermanable: massive reduction of surface area from up to several hundred $\frac{m^2}{g}$ in porous ASW to less than one $\frac{m^2}{g}$ in compact ASW
- Pore diameters less than 21 \AA \rightarrow micropores
- decline in microporosity at $90\text{-}130 \text{ K}$, suggested to be preceded by pore clustering at $< 90 \text{ K}$
- Most often a spherical nature of pores is suggested \rightarrow wrong
- Power-law scattering below 1 \AA^{-1} arises mainly from grain surfaces, above $0,1 \text{ \AA}^{-1}$ mainly from microporosity

Previous works:

- samples prepared similarly to the ones used here were characterized by calorimetry, dielectric relaxation, BET isotherms using N_2 as adsorption gas, IR spectroscopy, and diffraction (Innsbruck)
- \rightarrow BET surface area of all samples before pore collapse is $\approx 220 - 240 \frac{m^2}{g}$
- Boke et al.: electron scanning microscopy
 - observed small amorphous particles ($0,2$ to $0,4 \mu\text{m}$) in amorphous solid water films
 - Temperature: 90 to 123 K
- \rightarrow particles increase to $\sim 1 \mu\text{m}$ after crystallization
- Hass et al.: interference peaks in $I(Q) \cdot Q^3$ vs. Q plots (pseudopeaks) hint at periodic spacings

This work:

- granularity:
 - SANS signal remains strong after crystallisation
 - it must contain other contributions than only micropores \rightarrow granules
 - length of granules up to few mm, diameter $\approx 0,5 \text{ mm}$
 - change in surface roughness with temperature, especially upon crystallization ($Q < 0,03 \text{ \AA}^{-1}$ \rightarrow Porod exponent increases with T from 3 to almost 4, $0,1 \text{ \AA}^{-1} < Q < 0,3 \text{ \AA}^{-1}$: Porod exponent = 4 const. for all T)

- crystallization:

- all samples crystallise at same temperature (disappearance of "knee")
- flattening of SANS signal not due to crystallisation but to morphological changes / or pore-collapse in ASW

- pseudo-periodicity of micro pores:

- in $I(Q) \cdot Q^{2.5 \pm 0.3}$ vs Q plots, "knee" shows as "pseudo-peak"
- peak position gives information about length scale of pseudo periodicity
- $d = \frac{2\pi}{Q}$, changes between 60 and 77 Å for ~~baffled~~ baffled samples, stable at 70 Å for non-baffled samples
- knee does not shift significantly with $T \rightarrow$ no big size change of pores

- pore structure change:

- flattening of knee indicates shape change with T
- competition between pore-clustering and pore-collapse
- pore collapse becomes dominant at higher T (140 / 130 K for non-/baffled samples)

- comparison of baffled and non-baffled samples:

- deposition ~~rate~~ method does not influence results significantly
- deposition method influences stability of pore structure critically
- non-baffled samples seem to have higher stability against pore collapse and shape change
- baffled flow: mainly deposition of water monomers on surface (flat ASW samples)
- non-baffled flow: deposition of water-oligomers may be more important (tower-like structures \rightarrow stalactites)
- more experiments and simulations needed to understand why stalactites are more stable)

non-baffled samples

$$\xleftarrow{3D \text{ micropores}} s=1, R_G = 15\text{\AA}$$

$$\xleftarrow{2D \text{ micropores}} s=2, R_G \approx 10\text{\AA}$$

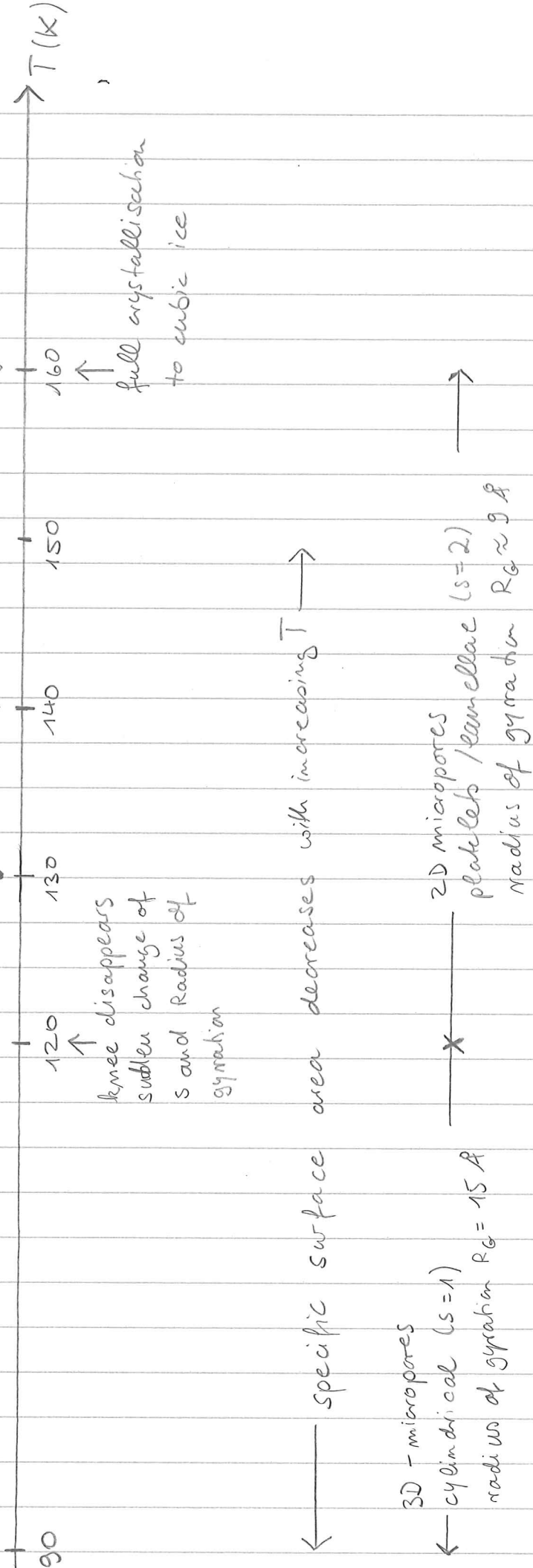
specific surface area increases with increasing T

specific surface area decreases with increasing T

radius of gyration stable over 1 hour

knee disappears sudden change of s and Radius of gyration

full crystallisation to cubic ice



baffled samples

Comparison with previous works:

- specific surface areas agree well BET results for baffled samples, but are lower than BET results by a factor of 2 to non-baffled samples. (BET : $230 \frac{m^2}{g_{\text{mm}}}$)
- increase of specific surface area for non-baffled samples below $T = 120\text{ K}$ may be attributed to pore clustering (as suggested by Wu et al.)
- similar cylindrical to lamellar transition found in poloxamer Pluronic P85 ($\text{EO}_{26}\text{PO}_{40}\text{EO}_{26}$) in deuterated water
- sudden 3D to 2D transition, preceded by gradual specific surface area reduction and/or pore-clustering
- other works also observed gradual nature over broad temperature range, but not the sudden transition
- maybe sudden pore collapse can not be inferred easily by e.g. observing the dangling OH modes.